International Journal of Engineering Trends and Technology
ISSN: 2231-5381/ https://doi.org/10.14445/22315381/IJETT-V74I7P120

Volume 74 Issue 7, 310-327, July 2026

Original Article

Frequency Control and Power Efficiency in Virtual Power Plants Using Novel Self-Adaptive Siberian Tiger Optimization for Fractional Order PID Controllers

Srinivasa Rao.Sureddy[1*], Nageswara Rao Pulivarthi[1]

[1]*Department of EECE, GITAM Deemed to be University, Visakhapatnam, Andhra Pradesh, India.*

[1*]*Corresponding Author : ssureddy2@gitam.in*

Received: 26 March 2026 Revised: 12 June 2026 Accepted: 18 June 2026 Published: 28 July 2026

***Abstract** - The increasing integration of renewable energy sources has significantly reduced greenhouse gas emissions and mitigated global warming. However, maintaining stability and efficient power management in Virtual Power Plants (VPPs) under dynamic operating conditions remains a major challenge. This study proposes a Self-Adaptive Siberian Tiger Optimization (SA-STO) based hybrid Proportional Integral–Fractional Order PID (PI-FOPID) controller for enhancing frequency regulation and power efficiency in VPP systems integrating solar photovoltaic systems, wind turbines, energy storage systems, diesel generators, and electric vehicles. The proposed hybrid controller combines the fast response of PI control with the robustness and flexibility of FOPID control, while the SA-STO algorithm optimally tunes controller parameters to improve system performance. MATLAB/Simulink simulations are conducted to evaluate the proposed approach against conventional PI, PID, and FOPID controllers using performance metrics such as frequency stability, overshoot response, power loss, and Total Harmonic Distortion (THD). The simulation results demonstrate that the proposed SA-STO-based hybrid PI-FOPID controller achieves enhanced dynamic response, improved stability, and reduced harmonic distortion, with a THD of 3.74%, compared with conventional controllers.*

***Keywords** - VPP, Renewable energy, Frequency control, Metaheuristic optimization, and FOPID controller.*

1. Introduction

A Virtual Power Plant (VPP) has emerged as an effective solution for integrating multiple types of DERs (for example, solar PVs, wind turbines, Battery Energy Storage Systems (BESSs), diesel generators, and electric vehicle charging stations) into one controllable framework that can be used in market-related activities (for example, electricity markets) and to provide ancillary services to the grid [1, 2]. By aggregating these heterogeneous resources through advanced energy management systems, allowing for coordinated dispatch (the scheduling of production from different resources) of energy resource generation, thereby decreasing reliance on fossil-fuel generation and positively impacting grid reliability through increased renewable power generation [3]. As energy systems around the world move towards decarbonization targets, VPPs will play an essential role in enabling future power systems to operate reliably, flexibly, and sustainably, even at high levels of renewable penetration. However, maintaining stable and optimal frequency regulation in VPPs presents a critical technical challenge. Renewable energy generation from wind and solar PV is inherently variable and intermittently created; therefore, they create continuous power imbalances due to their inherent characteristics, nonlinear dynamics, harmonic distortion, and propagation delay throughout the entire VPP structure [4]. These disruptions in the VPP can lead to extreme frequency deviations that can lead to loss of grid stability and power quality if not properly controlled. Unlike traditional, centrally planned generating plants that control frequency regulation using conventional monitoring systems, VPPs use geographically distributed DERs connected via wide area communication networks in which there are significant time delays and uncertainty due to the nature of communications to degrade the performance of the controller [5, 6]. In VPP technologies, there are many challenges to achieving stable and optimal frequency regulation when interfacing with renewable power due to variability in renewable electricity resources such as wind and PV generation, which creates nonlinear variations and introduces noise resulting from propagating delays, harmonic distortion, and power imbalances throughout the VPP structure [4]. Existing optimization methods like PSO, GOA, SSA, and ANN-based approaches include high computational complexity and long convergence times, low adaptability, and poor resilience to changing loads or disturbances [7, 8]. Similarly, the traditional PI Controller, PID Controller, and Fractional Order PID (FOPID) Controllers cannot effectively manage the effects of unknown conditions and nonlinear system behavior that characterize modern VPP systems [9]. To overcome these limitations, this paper proposes a novel Self-Adaptive Siberian Tiger Optimization (SA-STO) based hybrid PI-FOPID controller to enhance the frequency and enhance the efficiency of Virtual Power Plant (VPP) applications. Unlike conventional optimization algorithms, the proposed SA-STO provides adaptive chaotic prey and bear hunting strategies to assist global exploration and local exploitation to optimize the tuning of control parameters for the hybrid PI-FOPID controller compared with using conventional optimization procedures. A hybrid PI-FOPID controller combines the rapid transient response of PI control with the greater robustness and flexibility of FOPID control to help account for the variability of renewable energy sources. This system aims to diminish the frequency deviations, lower THD, minimize power loss, and enhance VPP stability for the entire range of potential VPP operating capabilities. The primary contributions and novelties of the proposed system are described as follows:

- A Virtual Power Plant (VPP) framework integrating Distributed Energy Resources (DERs) such as solar photovoltaic systems, wind turbines, Energy Storage Systems (ESS), diesel generators, and electric vehicles is developed to enhance renewable energy utilization and grid stability.
- A hybrid Proportional Integral–Fractional Order Proportional Integral Derivative (PI-FOPID) controller is proposed to improve frequency regulation, dynamic response, and power management performance in VPP systems under varying operating conditions.
- A novel Self-Adaptive Siberian Tiger Optimization (SA-STO) algorithm is employed for optimal tuning of the hybrid PI-FOPID controller parameters to enhance convergence behaviour, reduce power losses, and minimize Total Harmonic Distortion (THD).
- The effectiveness of the proposed SA-STO-based hybrid PI-FOPID controller is validated using MATLAB/Simulink through comparative analysis with conventional PI, PID, and FOPID controllers in terms of frequency stability, overshoot response, power loss, and THD performance.

The structure of the paper is as follows: In Section 2, a summary of relevant literature is given. Section 3 explores the proposed Strategy. Section 4 examines the results. The conclusion of the paper is found in Section 5.

2. Literature Survey

Srivastava et al., [10] investigated a wind power source, an electric car, and a parabolic dish solar collector heater associated with a synchronized control grid. The research examined an active method to manage energy with respect to communication latency in an interconnected microgrid. They utilized two-level controllers as well as a proportional-integral control strategy and applied various methods (PSO, Firefly Algorithm, Butterfly Optimization, and Grasshopper Optimization Algorithm [GOA]) for tuning of their parameters. The data collected showed that the GOA algorithm produced superior results compared to all other types of optimization techniques and exhibited greater resiliency for parametric variations within an integrated Virtual Power Plant (VPP) model. However, this method has the potential for increased computational complexity and very little flexibility when dealing with rapidly changing renewable energy sources, which can negatively affect real-time frequency regulation performance within today's modern VPP systems. Abdolrasol et al., [11] examined the implementation of Artificial Neural Networks (ANN) as intelligent controllers in VPP in a microgrid using ANN-BBSA and ANN-BPSO techniques. Improvements were observed in system efficiency, carbon dioxide (CO_2) emissions, and fuel consumption in various operating conditions with this approach. Improvements were made to the scheduling performance of the virtual power plant; however, many computational resources would be required, and the approaches relied heavily on the quality of training, thereby limiting applicability to real-time VPP systems. Abishek et al.,[12] established a frequency control for VPP systems using PI and FOPID controllers that were optimized through various metaheuristic algorithm methods such as SSA, PSO, Firefly, and Grasshopper Optimization. Improvements to frequency regulation performance were achieved with these techniques regardless of communication delays or variability in the operating conditions of the virtual power plant. However, the performance of the optimization methods suffered from slower convergence and less robustness because of varying degrees of nonlinear fluctuations in renewable energy sources used by the VPP system.

Chen et al.,[13] suggested a cooperative bidding strategy for VPPs with PV-BESS systems, Frequency Control Ancillary Service (FCAS) markets, utilizing the Nash-Harsanyi Bargaining Solution. The model's cooperation income allocation and battery utilization efficiency were improved. Simulation results confirmed that the bidding strategy used to provide VPPs with an increased opportunity to participate in power market auctions was feasible. Therefore, the focus of the methodology is more about maximizing economic optimization, with less consideration of frequency stability and dynamic control performance of VPP systems.

Bao et al.,[14] created a system for High-Voltage Direct Current (HVDC) power assistance using a distributed Model Predictive Control (MPC) for industrial VPP applications with significant renewable energy penetration levels – to enhance grid-support capabilities. The system improves secondary frequency control and optimizes EDCPS capacity in value-added functions over Time. However, while successfully supporting the grid, the MPC structure creates greater computational complexity in terms of control implementation for VPPs executing real-time operations. Ali et al., [15] proposed a multi-objective real-time Energy Management System (EMS) for VPP using AMO-Grey Wolf Optimisation (AMO-GWO), Hybrid Particle Swarm Optimisation (H-PSO), and Hybrid Oppositional Swarm Residuals (H-OSR). The purpose of this approach is to diminish the operating cost, emissions, and improve the load schedule and customer satisfaction. The AMO-GWO algorithm achieved better optimization performance compared with the H-PSO and H-OSR methods. However, the results indicated that the optimization techniques were less adaptive to highly variable and dynamic renewable energy generation supply conditions and thus placed high computational demands on the EMS. Borisoot et al.,[16] introduced a novel energy management framework for VPP systems that incorporated solar PVs and EVCS. The energy management framework is optimized by using the Differential Evolution (DE) optimization method and leads to the minimization of generation operating costs and maximizing optimal power flow performance in the IEEE 24 bus Reliability Test System. This research demonstrates the effectiveness of utilizing the DE optimization method to reduce the number of operation violations; however, the DE method is computationally complex and has limited adaptability when working with dynamic renewable energy sources. Lamari et al.,[17] designed an improved Particle Swarm Optimization (PSO) based Multi-Objective Energy Management System (MOEMS) for VPP applications that utilize Distributed Energy Resources (DERs), including photovoltaic systems, wind power generation, battery storage, and micro-turbines. The proposed MOEMS led to reductions in operating costs and greenhouse gas emissions across multiple operating scenarios; however, the PSO-based optimization approach did experience issues with premature convergence and a lack of robustness in the presence of distributed nonlinear VPP operating conditions. Pal et al., [18] proposed a smart energy management framework using IoT and PLCs to enhance energy utilization and operational profit in VPP systems by accounting for variable loads. The research demonstrates multi-faceted smart energy management across numerous operating conditions; however, it was primarily focused on the economic management of the VPP system while offering limited consideration for frequency stability and harmonic distortion due to renewable sources' interconnection to that system. Häberle et al.,[19] developed a multi-objective optimization framework for VPP systems based on probabilistic forecasting and the use of hybrid swarm optimization techniques in order to minimize emissions and voltage variations while maximizing operational profit. Enhanced flexibility and reduced uncertainty associated with VPP operations were demonstrated using their proposed method. However, the additional complexity of the optimization and increased computational burden could potentially hinder real-time implementation of the framework within larger VPP systems. Table 1 illustrates the summary of the literature review.

Table 1. Summary of literature review

Author	Method	Advantage	Disadvantage
Srivastava et al., (2022)	Synchronized control with optimization algorithm	Superior optimization.	Integration complexity
Abdolrasol et al., (2023)	ANN-based controllers	Improves efficiency	Complex to implement in practice.
Abishek et al., (2023)	Frequency control with optimization	Effective for diverse energy resources	Slow response
Chen et al., (2022)	Optimal bidding strategy with payoff allocation	Maximize cheers participation	Complex to execute and verify
Bao et al., (2022)	Secondary frequency control using MPC	Addresses renewable integration issues	Requires significant infrastructure
Ali et al., (2022)	Real-time smart energy management with multiple optimization algorithms	Optimal scheduling and efficient management	Real-time implementation challenges
Borisoot et al., (2022)	Optimal energy management with DE for PVs and EVCS	avoids constraint violations	Limited generalizability of consequences
Lamari et al., (2022)	Multi-objective particle swarm optimization for scheduling.	Maximize validated scenarios	Algorithm complexity
Pal et al., (2021)	Smart management using PLCs and IoT.	Optimize profit margins	Integration of PLCs and IoT is complex
Li et al., (2024)	Probabilistic prediction-based optimization framework	Improves efficiency and flexibility	High computational complexity

2.1. Research Gap

Although several optimization and control strategies for VPP, many of the currently available techniques have problems such as higher computational loads, getting stuck in local minima, lack of robustness and adaptability when dealing with the volatile nature of renewable energy sources, etc. Furthermore, most of the currently employed schemes tend to focus more on the economic optimization aspect of the operation of the VPP than on other important aspects, such as the ability to maintain frequency stability, reduce harmonic distortion, and maintain the dynamic control performance of the VPP. Therefore, to address these issues, this study introduces a Self-Adaptive Siberian Tiger Optimization (SA-STO) based hybrid PI-FOPID controller for improving frequency control, reducing Total Harmonic Distortion (THD) and power losses, and increasing overall system stability in VPP systems with varying operational conditions.

2.1.1. Proposed Methodology

Distributed Energy Resources (DERs) such as solar PV, wind turbines, ESS, and Electric Vehicles are introduced in VPPs systems, because of the intermittent characteristics of renewable energy sources. Therefore, a SA-STO-basedHybrid PI-FOPID Controller for Frequency Regulation and Power Management for VPP Applications. The SA-STO Algorithm will optimally tune the PI-FOPID Controller parameters through adaptive prey hunting as well as Bear Fighting Strategies and Chaotic Mapping to improve the global exploration and local exploitation capabilities of the proposed Strategy. By exploiting the capabilities of the SA-STO Algorithm, frequency deviation reductions, lower Total Harmonic Distortion (THD), reduced power losses, and quicker convergence rates will be achieved. Figure 1 illustrates the overall framework of the proposed system.

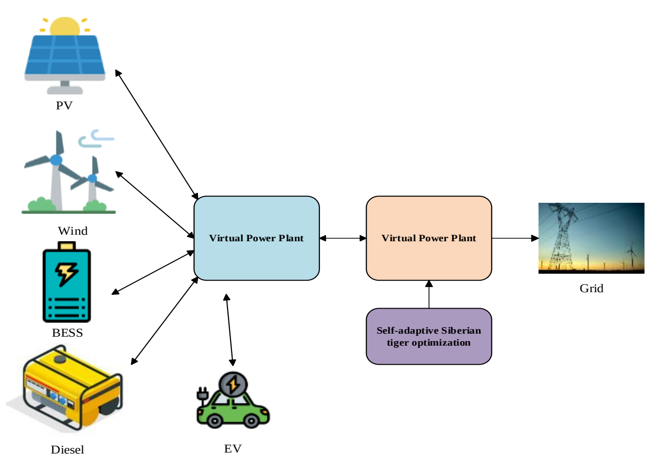

Fig. 1 Architecture of the proposed system

Photovoltaic generation

PV is the best substitute for using solar energy to generate electricity without producing greenhouse gases. Among the many renewable resources, it has a long lifespan, good efficiency, low maintenance, sturdiness with long lifespan. The PV system consists of series-connected cells that generate the required voltage. The PV plane of the ultimate output voltage estimate is obtained by multiplying the output current by the terminal voltage. In Figure 2, the PV panel's built model is shown.

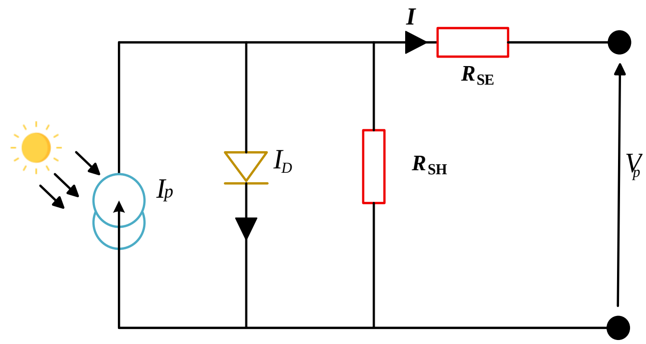

Fig. 2 PV model

The PV panel terminal and current voltage for design is calculated using Equations (1) and (2).

$$I_p = I_{SC} - I_O\left\{\exp\left[\frac{Q}{akt}\left(V_p + I_p R_{SE}\right) - 1\right]\right\} - \frac{V_p + I_{SC}R_{SE}}{R_{SH}} \tag{1}$$

$$V_p = \frac{akt}{Q}\ln\left\{\frac{I_{SC}}{I_p} + 1\right\} \tag{2}$$

Where Q is the electron charge, t is the temperature in Kelvin, k is the Boltzmann constant, R_{SH} and R_{SE} are the shunt and series resistances, V_p is the PV voltage, and I_{SC}denotes the short-circuit current. The power produced by the PV is computed as (3)

$$P_{PV}(t) = N_{pv}(t) \times I_{pv}(t) \times V_{pv}(t) \tag{3}$$

Where $N_{pv}(t)$ is the number of the PV array, $I_{pv}(t)$is the PV current, and. P_{PV} is the PV voltage.

Wind Turbine (WT)

The wind speed follows the Weibull Distribution function, and the PDFThe wind speed is given by Equation (4),

$$f_w(v) = \left(\frac{s}{\gamma}\right)\left(\frac{s}{\gamma}\right)^{s-1} e^{-\left(v/\gamma\right)^s} \tag{4}$$

Here v is the actual wind speed, s is the shape factor, γ is the scaling factor. The WTThe outputpower is given by Equation (5),

$$P_{wt}(v) = \begin{cases} 0, & v_{c-in} > v > v_{c-out} \\ \frac{v - v_{c-in}}{v^* - v_{c-in}} P_r, & v_{c-in} \leq v < v_r \\ P_r, & v_r \leq v < v_{c-out} \end{cases} \tag{5}$$

Where, $v_r P_r$, are the rated wind velocity and power of WT. v_{c-in}&v_{c-out} are the cut-in and cut-out wind speeds. The PDFThe WT power output is given by Equation (6),

$$f_o(P_{WT}) = \begin{cases} \left(\frac{skv_{c-in}}{\gamma P_r}\right)\left((1+kP_{WT}/P_r v_{c-in})/\gamma\right)^{s-1} \\ \times e^{\left\{-\left[\frac{\left(\left(1+\frac{kP_{WT}}{P_r}\right)v_{c-in}\right)}{\gamma}\right]^k\right\}} & P_{WT} \in [0, P] \\ 0, & otherwise \end{cases} \quad (6)$$

here $k = \left(\frac{v_r}{v_{c-in}}\right) - 1$

BESS

ESS plays a vital role in reducing frequency deviations caused by renewable generation fluctuations. The rating of an ESS is affected by several factors, and the battery's charging and discharging schedule is given by Equation (7),

$$P_{BES}(t) = \begin{cases} P_{ch}(t), if\ P_{PV}(t)+P_{WT}(t)+P_{DG}(t) \\ +P_{FC}(t)+P_{MT}(t)+P_g(t)-P_d(t) \geq 0 \\ P_{dc}(t), if\ P_{PV}(t)+P_{WT}(t)+P_{DG}(t) \\ +P_{FC}(t)+P_{MT}(t)+P_g(t)-P_d(t) < 0 \end{cases} \quad (7)$$

Let, $P_{BES}(t)$- output power of the battery energy storage system,
$P_{ch}(t)$- charging power of the battery,
$P_{dc}(t)$- discharging power of the battery,
$P_{PV}(t)$- photovoltaic output power,
$P_{WT}(t)$- wind turbine output power,
$P_{DG}(t)$- diesel generator output power,
$P_{FC}(t)$- fuel cell output power,
$P_{MT}(t)$- microturbine output power,
$P_g(t)$- grid power
$P_d(t)$- load demand power.

A BES system can only operate in a single mode, either charging or discharging. The battery's charging and discharging power is given by Equations (8-11):

$$E_{ch}(t) = \left(\frac{P_{WT}(t)+P_{DG}(t)+P_{FC}(t)+P_{MT}(t)-P_d(t)}{\eta_{conv}} + P_{PV}(t)\right) * \Delta t * \eta_{ch} \quad (8)$$

$$SOC(t) = SOC(t-1)(1-\rho) + E_{ch}(t) \quad (9)$$

$$E_{dc}(t) = \left(\frac{-P_{WT}(t)-P_{DG}(t)-P_{FC}(t)-P_{MT}(t)+P_d(t)}{\eta_{conv}} - P_{PV}(t)\right) * \Delta t * \eta_{dc} \quad (10)$$

$$SOC(t) = SOC(t-1)(1-\rho) - E_{ch}(t) \quad (11)$$

Where, $E_{ch}(t)$ refers to the charging energy of the battery, $E_{dc}(t)$ is the discharging energy of the battery, $SOC(t)$ denotes the state of charge of the battery at Time t, ρ represents the self-discharge rate of the battery, η_{conv}, η_{ch}, and η_{dc} are the converter, charging, and discharging efficiency, Δt is the sampling time interval. Factors that affect the lifetime of a battery storage system are throughput capacity and float life. If a battery storage bank reaches its maximum capacity, it must be replaced. The lifetime of a storage bank is determined by the Equation given in (12).

$$B_{SBL} = \begin{cases} N_{bat}Q_{lifetime,}\ for\ throughput\ limit \\ B_{SBLf},\ for\ time\ limit \\ min\left(\frac{N_{bat}Q_{lifetime,}}{Q_{throughput,}}, B_{SBLf}\right), for\ throughput \\ and\ time\ limit \end{cases} \quad (12)$$

Here, B_{SBL}- battery storage bank lifetime,
N_{bat}- Number of Batteries,
$Q_{lifetime}$- battery lifetime throughput,
$Q_{throughput}$- total throughput of the battery bank,
B_{SBLf}-float life of the battery storage system.

The float life of a storage system represents its usable duration before replacement, and the choice to limit its lifespan can be based on Time, throughput, or both. If the storage lifetime is solely determined by throughput, the float life concept is not applicable.

Diesel generator

Biodiesel Generators (BDGs), which resemble natural diesel, even though they are made from low-maintenance energy crops. It can be used in many different ways, even in its purest form (B100). The BDG output power's linearized model can be roughly represented as follows: Equation (13).

$$\Delta P_{BDG} = \frac{k_{VA}}{1+ST_{VA}} \times \frac{k_{BE}}{1+ST_{BE}} \quad (13)$$

WhereΔP_{BDG} is the output power of the BDG,k_{VA}, T_{VA}, k_{BE}, and T_{BE} are the valve gain, valve actuator delay, engine gain, and time constants of the BDG.

Plug-in Hybrid Electric Vehicle

PHEVs connect to the centralized VPP control system via an Energy Management System (EMS); that communication occurs over a Wide Area Network (WAN), and practical VPP operations will necessarily have some transmission delay that is beyond the control of the operator. Because there is communication delays related to the WAN and transmission delays during the Time it takes for messages to be relayed from the EMS to each PHEV, it is necessary to model the delays using the following first-order Pade approximation, which is given in Equation (14),

$$G_{EV} = \frac{K_{EV}}{1+sT_{EV}} \quad (14)$$

Load and Machine Dynamics of VPP

Any imbalance in power inside the system causes frequency variations. The independent area of VPP's net power imbalance at any given time can be shown as in Equation (15),

$$\Delta P_e = (P_{PV} + P_{PW} + P_{BES} + P_{EV}) - P_{d1} \quad (15)$$

The transfer function, as follows, represents the change in frequency brought about by a change in net power in Equation (16).

$$G_{sys} = \frac{\Delta f}{\Delta P_e} = \frac{1}{Ms+D} \quad (16)$$

Based on the damping coefficient of the loads (D) in the system and the moments of inertia (M) of the spinning mass in the system, the frequency was altered.

The VPP controlling the grid has a centralized strategy that employs ICT for monitoring and controlling power flow and frequency deviations. The EMS collects data from all the Distributed Energy Resources (DERs), which is then sent to the central VPP controller via a Wide Area Network (WAN), where the controller generates appropriate control signals to maintain system stability and frequency control based on the received operating conditions.

However, all the DERs are geographically distributed, and communication delays are unavoidable in the control loop. Therefore, a first-order Pade approximation is incorporated to model the communication delay in the VPP control system, which is mentioned in the given Equation (17).

$$e^{-sT_D} = \frac{-\frac{1}{2}sT_D+1}{\frac{1}{2}sT_D+1} \quad (17)$$

The demand for a more dependable and adaptable controller arises with system complexity.

Hybrid PI-FOPID controller

The hybrid PI-FOPID controller is intended to control variations in frequency and tie line power in the VPP under changing renewable energy and load disturbance conditions. The PI controller will quickly respond to disturbances and reduce steady state error, while the FOPID controller will improve system dynamics and stability through fractional order control techniques. The output of the PI controller is made to be an input reference for the FOPID controller. This will further improve frequency regulation performance when dealing with nonlinear and uncertain operational conditions. The controller parameters are optimally tuned with the SA-STO algorithm for the minimization of power loss as well as the improvement of overall VPP stability. The configuration of the hybrid PI-FOPID controller is shown in Figure 3.

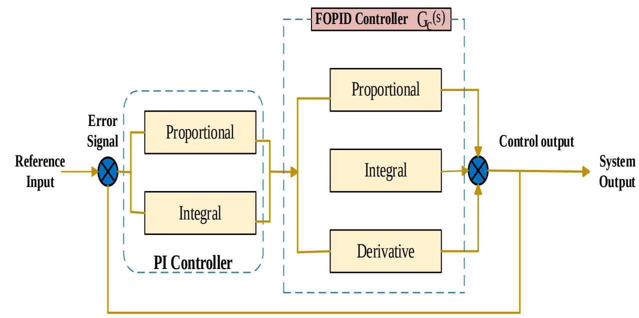

Fig. 3 Hybrid PI-FOPID controller

PI controller

The reference input $R(s)$ defines the system frequency or power output, while $Y(s)$ is the actual system output of the VPP, and $E(s) = R(s) - Y(s)$denotes the error signal that the controller seeks to minimize to stabilize the system. To begin, the PI controller will process the error signal in order to achieve a more desirable transient response of the system and reduce the error at steady state. The proportional gain (K_p) of the PI controller improves rise time, while the integral gain(K_i) reduces steady-state error. The total output of the PI controller is as Equations (18-19).

$$C_{PI}(t) = K_p(t)e(t) + K_I(t) \quad (18)$$

$$U_{PI}(s) = K_{p1}E(s) - \frac{K_I1}{s}E(s) \quad (19)$$

Where $K_i(t)$ is the integral gain and $K_p(t)$ is the proportional gain, and $e(t) = \omega_r^*(t) - \omega_r(t)$. These improvements depend on the speed error e(t). As a function of speed error, the gain $K_p(t)$ is expressed in Equation (20):

$$K_p(t) = K_{p(max)} - \left(K_{p(max)} - K_{p(min)}\right)e^{-[ke(t)]} \quad (20)$$

Where the rate at which $K_p(t)$ differs between the minimum and maximum values of the proportional gain is determined by a constant, k. When the speed error $e(t)$ is large, a large proportional gain, $K_{p(max)}$, is employed to quicken the transient response; when the error $e(t)$ becomes small, at least proportional gain, $K_{p(min)}$, is used to eradicate oscillations and overshoots. The integral gain in relation to the speed error signal $e(t)$, $K_i(t)$ is expressed in Equation (21):

$$K_i(t) = K_{i(max)}e^{-[ke(t)]} \quad (21)$$

When the speed error $e(t)$ is small under steady state conditions, a high integral gain is employed to compensate for the steady state error. To eliminate the unwanted oscillations and overshoot, a small integral gain is employed when the error is high. In a transient condition, the motor is accelerated or decelerated to the reference value in the shortest amount of Time possible using a large control signal. $K_p(t)$ reaches its highest value and $K_i(t)$ stays at its minimum value during this Time. When operating in a steady state, the integral gain $K_i(t)$ increases to its highest.

FOPID controller

A Fractional Order PID (FOPID) controller is used as the second control block to extend the functionality of the traditional (integer order) version of the PID controller via fractional calculus. With its non-integer (i.e., fractional) powers for defining the integration and derivative terms, the FOPID offers additional flexibility and robustness than those of traditional (integer order) PID controllers to accommodate for nonlinear dynamic behavior, time-lags, and uncertainty in VPP systems. Due to its better dynamic response and greater stability characteristics, the FOPID controller is widely used in applications related to renewable energy. Gain of the controller and the transfer function are given by Equations (22) and (23).

$$C_{FOPID}(t) = K_P + K_I \frac{1}{s^{\lambda}} + K_D s^{\mu} \tag{22}$$

$$U_{FOPID}(s) = K_{p2}E(s) + \frac{K_I 1}{s^{\lambda}} E(s) + K_{D2} s^{\mu} \tag{23}$$

Where $Y(s)$ and $U(s)$ represent the output and input (error) to the controller, respectively, and Gc is the controller's transfer function. The fractional parts of the integral and derivative controllers with corresponding gains, denoted as K_I and K_D, respectively, are represented by λ and μ in (21). K_P also stands for proportionate gain. The error between the desired and actual values is represented by $U(s)$. The PI controller focuses on minimizing initial large errors, and later on, the FOPID takes over to refine the response by its advanced fractional-order dynamics.

The fractional parts make the controller very robust with the delays and non-linearities of the system, better than the usual PID controller. When compared to ordinary integer-order controllers, the fractional-order terms (s^{μ} and s^{λ}) give more versatility. Because of this, FOPID controllers are more suited for complicated dynamical systems with renewable energy sources, such as VPPs. Specifically, the FOPID controller improves the capacity to manage the uncertainties and non-linearities present in the production of renewable energy. The hybrid control system's output, denoted as $U(s)$, is the combined signal from the PI and FOPID controllers. This signal is then supplied into the system VPP to alter its behaviour and bring the real output $Y(s)$closer to the desired reference input $R(s)$as represented in Equation (24).

$$U(s) = U_{PI}(s) + U_{FOPID}(s) \tag{24}$$

To ensure optimal performance of the hybrid controller, it is necessary to optimize the following parameters: $K_{P1}, K_{I1}, K_{P2}, K_{I2}, K_D, \lambda$, and μ. To determine the ideal values for these parameters, the Self-Adaptive Siberian Tiger Optimization (SA-STO) algorithm is employed in this work. The overall objective is to reduce the losses in the VPP by tuning the parameters of the FOPID controller via the SA-STO algorithm. It also guarantees efficient use of renewable sources as well as stability within the system at large. As a result, there are impacts on tie-line power deviations, which result in the reduction of those power losses. The objective function for power loss minimization as follows in Equation (25).

$$\min P_{loss} = f(K_P, K_I, K_D, \lambda, \mu) \tag{25}$$

It is subjected to

$$\begin{gathered} K_P^{min} \le K_P \le K_P^{max} \\ K_I^{min} \le K_I \le K_I^{max} \\ K_D^{min} \le K_D \le K_D^{max} \\ 0 \le \lambda \le 2 \\ 0 \le \mu \le 2 \end{gathered}$$

The controller's parameters, K_P, K_I, K_D, λ, and μ are adjusted by the optimization SA-STO to reduce power losses.

Self-adaptive Siberian tiger optimization

The parameters of the hybrid PI-FOPID are optimized using a novel metaheuristic algorithm called Self-Adaptive Siberian Tiger Optimization (SA-STO). This algorithm simulates the two phases of prey hunting and bear combat, which are the natural hunting and survival methods of Siberian tigers. During the optimization, the tigers are looking for the best solutions in the search space, allowing the adjustment of position according to the objective function values. Two stages make up the process of upgrading Siberian tiger positions in the STO, which is based on the animal's natural activities.

Initialization

The iterative process of the suggested STO, which makes use of the population's search ability, can provide a feasible solution to the problem. The STO population, consisting of Siberian tigers, roams the search space for better solutions. The STO population consists of every Siberian tiger. As a result, it offers a potential fix for the issue. Mathematical models of Siberian tigers can be created from vectors for each individual and from matrices for the population, as shown in Equation (26). Its location within the search area indicates values for the problem's variables.

$$ST = \begin{bmatrix} ST_1 \\ \vdots \\ ST_i \\ \vdots \\ ST_N \end{bmatrix}_{N\times m} = \begin{bmatrix} st_{1,1} & \cdots & st_{1,j} & \cdots & st_{1,m} \\ \vdots & \ddots & \vdots & \iddots & \vdots \\ st_{i,1} & \cdots & st_{i,j} & \cdots & st_{i,m} \\ \vdots & \iddots & \vdots & \ddots & \vdots \\ st_{N,1} & \cdots & st_{N,j} & \cdots & st_{1,1} \end{bmatrix}_{N\times m} \tag{26}$$

Let, the matrix X- population of Siberian tigers' locations,
x_i- i^{the} Siberian tiger (a candidate solution),
N- Total No. of Siberian tigers.

Under Sto, the initial random distribution of all of the tigers within the search area is accomplished by using the Stochastic Objective (STO) to generate their initial random locations using Equation (27),

$$ST_{i,j} = LB_j + r_{i,j}.(UB_j - LB_j), \quad i = 1,2,\dots,N; j = 1,2,\dots\dots,m \qquad (27)$$

where $r_{i,j}$- random values in [0, 1],

$X_{i,j}$ is the j^{th} dimension of ST_i in the search area (problem variable),

UB_j and LB_j- Each variable of upper and lower bounds,

m- total no. of variables.

Each tiger specifies the values of the problem variables that, after the optimizing process, give rise to an associated objective function value. These objective function values are collated into an objective function vector by implementing Equation 28 on all tigers' objective function values.

$$F = \begin{bmatrix} F_1 \\ \vdots \\ F_i \\ \vdots \\ F_N \end{bmatrix}_{N\times 1} = \begin{bmatrix} F(ST_1) \\ \vdots \\ F(ST_i) \\ \vdots \\ F(ST_N) \end{bmatrix}_{N\times 1} \qquad (28)$$

Where F_i is the attained objective function value for the ith tiger, and F is the objective function value vector.

Phase 1: Chaotic-based Prey Hunting

Strong predators, Siberian tigers hunt by attacking a diversity of prey. Therefore, in the initial stage, the STO members receive updates by mimicking the hunting tactics of Siberian tigers. This tactic involves the Siberian tiger first choosing its target, then attacking it and chasing it until it is killed. Thus, there are two steps of simulating the prey hunting phase.

The population's position is updated in the first stage according to the prey's attack and selection. This phase results in abrupt and significant shifts in the STO members' positions, which adjust the algorithm's capacity for global search and exploration and precise search space scanning. Every Siberian tiger in the STO design has recommended prey locations selected from among other members of the population whose objective function value is greater than that of that particular individual. The positions of these suggested prey are displayed in (29).

$$PPrey_i = \{ST_k | k \in \{1,2,\dots,N\} \wedge F_k < F_i\} \cup \{ST_{best}\} \qquad (29)$$

WhereST_{best}It is the best candidate solution. After that, the $i$the Siberian tiger (i.e., the $i$the population member) chooses at random one member of this set. $PPrey_i$ to attack, and Equation (30) is used to simulate the attack on the prey and compute its new location.

$$ST_{i,j}^{P1S1} = ST_{i,j} + r_{i,j}.(TP_{i,j} - I_{i,j}.ST_{i,j}) * Z_{i+1} \qquad (30)$$

$$Z_{i+1} = \cos(w * cos^{-1} z_i) - 1 \leq z_i \leq 1;\ w \in [2,6] \qquad (31)$$

where $I_{i,j}$ are random numbers from the set {1,2}. Z_{i+1} is the Chebyshev chaotic map, which is given in Equation (31). The Chebyshev chaotic map is used to introduce randomness and unpredictability into the attack simulation. It helps the algorithm to search different parts of the space and not get stuck in local optima. Additionally, ST_i^{P1S1} is the new location of the $i$the member based on the first stage of the first phase of STO, and $ST_{i,j}^{P1S1}$ is its $j$the dimension. If the new calculated position increases the value of the objective function, it is acceptable during the STO member update procedure. Equation (32) is used to model this process.

$$ST_i = \begin{cases} ST_i^{P1S1}, & F_i^{P1S1} < F_i \\ ST_i, & else \end{cases} \qquad (32)$$

where F_i^{P1S1}- i^{th} member

X_i^{P1S1}- objective function value.

In the second stage, the pursuit protocol updates the positions of the population members. At this point, the Siberian tiger adjusts its stance within the prey's vicinity, thereby enhancing the algorithm's effectiveness in local search and exploitation. The tiger's new location will be first determined using Equation (33) as it simulates the act of chasing, and subsequently should be compared to its prior location using Equation (34) to determine if the new position should be adopted.

$$ST_{i,j}^{P1S2} = ST_{i,j} + \frac{r_{i,j}.(UB_j - LB_j)}{t} \quad ; \quad t = 1,2,\dots.,T \qquad (33)$$

$$ST_i = \begin{cases} ST_i^{P1S2}, & F_i^{P1S2} < F_i \\ ST_i, & else \end{cases} \qquad (34)$$

Where t is the algorithm's iteration counter, $r_{i,j}$ are random integers in the interval [0; 1], F_i^{P1S2} is its objective function value, ST_i^{P1S2} is its jth dimension, and $ST_{i,j}^{P1S2}$ is the new location of the ith Siberian tiger based on STO's first phase's second stage. The flowchart of the SA-STO is shown in the Figure 4.

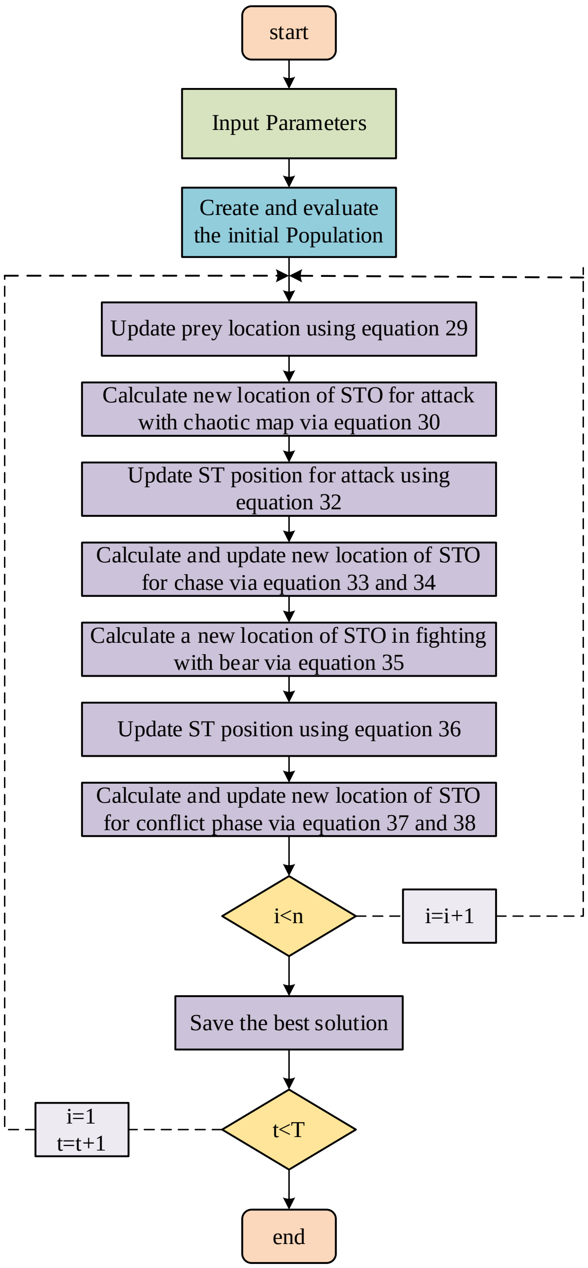

Fig. 4 Flowchart of SA-STO

Phase 2: Fighting with a Bear

In this stage, the SA-STO algorithm's fighting behavior of Siberian tigers is modelled to provide global exploration and solution updating improvements. Each tiger will randomly select one of the other tigers as a bear opponent, and will then change its position according to the combat strategy used by that tiger. Through this process, the position of each tiger is drastically changed from its previous location. There are advantages to this approach with respect to both the overall ability of the search process and to the potential for the algorithm to avoid becoming trapped in a local optimal solution. The calculation for determining the new position of the ith Siberian tiger is given by Equation (35).

$$ST_{i,j}^{P2S1} = \begin{cases} ST_{i,j} + r_{i,j.}(ST_{k,j} - I_{i,j}.ST_{i,j}), & F_k < F_i \\ ST_{i,j} + r_{i,j.}(ST_{i,j} - I_{i,j}.ST_{k,j}), & else \end{cases} \quad (35)$$

Let k is chosen at random from the set $\{1,2,\ldots.,i-1,i+1,\ldots,N\}$ and $X_{k,j}$ is the j^{th} dimension of a bear site, $j=1,2,..,m$. $X_{i,j}^{P2S1}$ represents the i^{th} member's new location according to the first stage of the second phase of STO; $X_{i,j}^{P2S1}$ is its j^{th} dimension; random numbers $r_{i,j}$ fall inside the interval [0; 1]; random numbers $I_{i,j}$ come from the set {1,2}. Therefore, if the new position produces a better (higher) objective function value, it replaces the member's old position as dictated by Equation (36).

$$ST_i = \begin{cases} ST_i^{P2S1}, & F_i^{P2S1} < F_i \\ ST_i, & else \end{cases} \quad (36)$$

where F_i^{P2S1}- objective function value of X_i^{P2S1}
F_k- objective function of the bear,
k^{th} member of STO.

In step 2, the members of the population will change their positions because of the battles that take place. This causes minor changes to the members' positions. This will help improve the local search and exploitation capability of the SOS algorithm. To simulate this behaviour, Equation (37) is first used to determine a random position close to the combat site.

$$ST_{i,j}^{P2S2} = ST_{i,j} + \frac{r_{i,j.}(UB_j - LB_j)}{t} \quad (37)$$

where t is the algorithm's iteration counter, $ST_{i,j}^{P2S2}$ is its jth dimension, and $ST_{i,j}^{P2S2}$ is the new location of the ith Siberian tiger, depending on the STO's second phase and stage. If the new position increases the objective function's value as per Equation (38), it is then appropriate for the update procedure.

$$ST_i = \begin{cases} ST_i^{P2S2}, & F_i^{P2S2} < F_i \\ ST_i, & else \end{cases} \quad (38)$$

Where F_i^{P2S2} is ST_i^{P2S2}'s objective function value. The proposed SA-STO algorithm effectively balances global exploration and local exploitation to obtain optimal controller parameters, thereby improving frequency stability, reducing power loss, and enhancing the overall performance of the VPP system.

3. Result And Discussion

This section analyses and evaluates the efficacy of the proposed method, SA-STO is currently under development for achieving control stability in VPP. The proposed framework has been implemented using the MATLAB- Simulink tool. The method was used with MATLAB with R2022a version and Windows 10 PRO.

The Intel® core (TM) i3-6098P CPU @ 3.60 GHz is the processor in use, and the total RAM is 8 GB. After a thorough trial and error process, the controllers' K_P, K_I and K_D parameters were determined to have upper and lower bounds between −1 and +1. Between 0 and 2, the fractional parameters λ and μ are selected. In order to minimize J, optimization algorithms were used to run the simulations up to a maximum of 200 iterations. The metrics analyzed include PV, wind and battery output, grid, power loss and THD. Then, the optimized PI- FOPID performance is compared with that of traditional FOPID, PID, and PI controllers. Figure 5 depicts the proposed Simulink model.

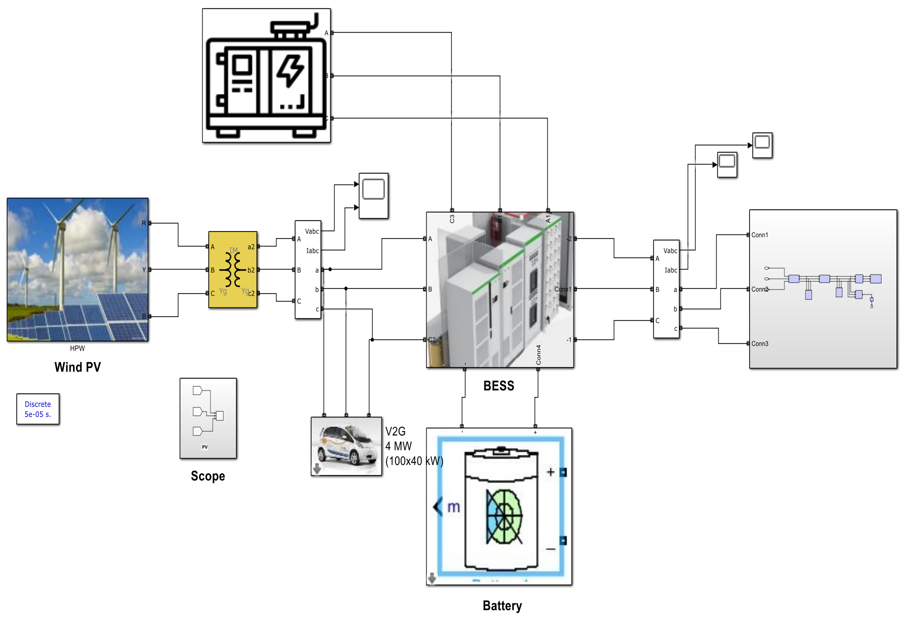

Fig. 5 The Simulink proposed model

3.1. Analysis of Wind Voltage Characteristics

Figure 6 represents the time series of wind generation output over a particular period, where it depicts how the power is generated in the fluctuations caused by changes in the wind speed

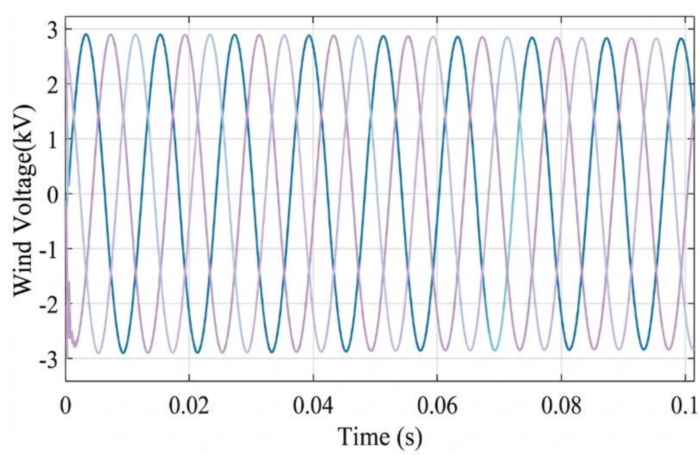

Fig. 6 Analysis of wind voltage fluctuation

As per the figure shows the three-phase wind generator voltage waveforms are plotted for a duration of 0.1 seconds. The three curves show that there are three different voltage levels produced by an AC generator. Each of these curves shows a smooth, sinusoidal waveform. The amplitudes of these waveforms are all about the same at three (3) kW, and these waveforms are 120° apart in phase. This indicates that the electrical generator system operates in a balanced, three-phase manner.

The frequency of these waveforms is also equal to approximately 50 Hz, the frequency of the power grid. The consistent and stable nature of the waveforms indicates steady wind speed during this period, with no visible spikes or disturbances.

3.2. Analysis of PV Output Power, Voltage, and Current

Figure 7 offers the output of PV generation as a function of Time, depicting time-of-day variability in solar energy production.

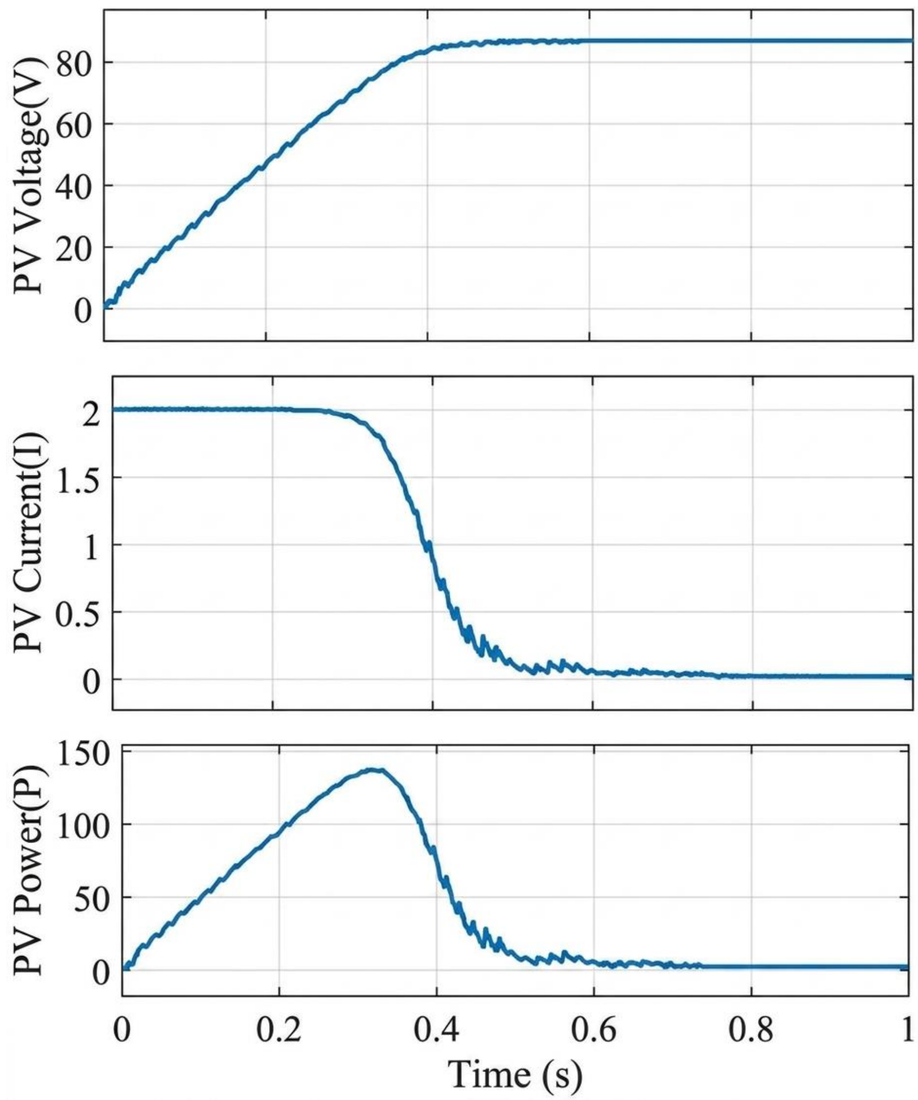

Fig. 7 PV output power, voltage, and current

As shown in the figure, the axis on x-axis is the Time across which the PV system was monitored, and the y-axis refers to power output, typically in Kilowatt-hours (kW) or Megawatts (MW), depending on the scale of the system.

A Solar PV (photovoltaic) system performance over a period of one second, along with three different plots of voltage, current, and power. The voltage starts at 0V and rises gradually to a stabilized level of approximately 85V.

The current remains steady at 2A for the first 0.3 seconds before dropping sharply to nearly 0A. As a result, the maximum output power is achieved at approximately 0.3 seconds (approximately 135W), then declines steeply with oscillations before settling close to 0W.

Overall, the Solar PV system operates normally for the first 0.3 seconds but then experiences a sudden disturbance (likely caused by either a decrease in solar irradiance or load demand), resulting in a drop in both current and power while the remaining voltage stays elevated.

3.3. Analysis of the Characteristics of Battery Voltage, Current, and SOC

Figure 8 offers the performance of the BESS inside the VPP.

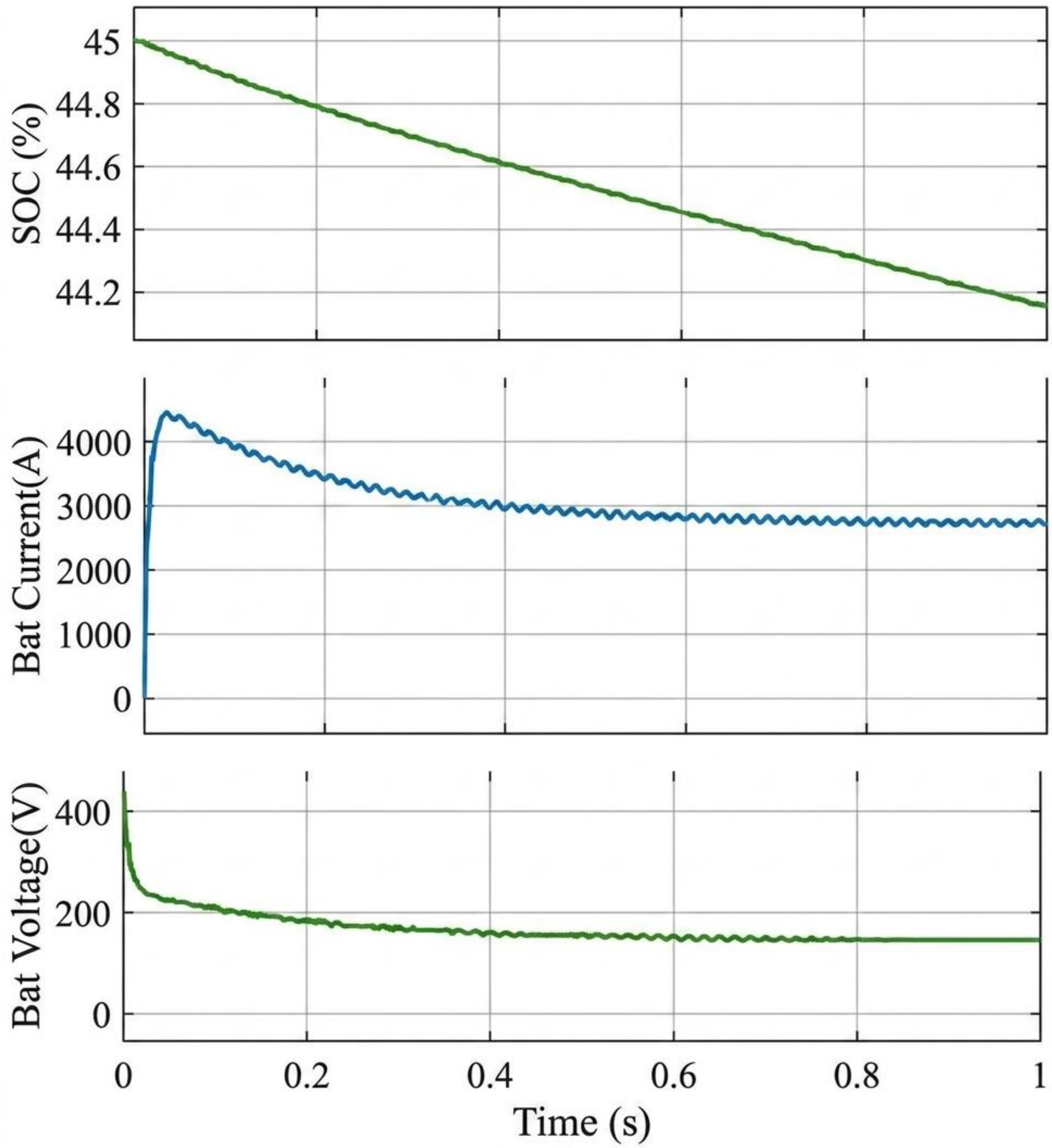

Fig. 8 Output of battery voltage, current, and SOC

The SOC plot shows the steady decrease of 44.8% over Time based on continuous battery discharge to supply the grid when there is not enough renewable energy available. The Battery Current data shows that the initial battery discharge current was around 4000 A and eventually stabilizes between 1500 and 2000 A. This indicates that the battery has undergone a controlled and stable discharge process. The Battery Voltage data has also gradually decreased from an initial (before discharge) voltage of 400 to below 220 V as a result of discharge and internal resistance.

The SOC data shows an increasing trend when charging the battery, with the charging current increasing from 0.2 to 0.6 A with a steady battery voltage at 220 V.

3.4. Analysis of the Characteristics of Grid Current

In the Figure 9, the analysis of grid voltage, the major characteristics were plotted against a graph where the x-axis depicts the time interval, while the y-axis denotes the current (A) levels.

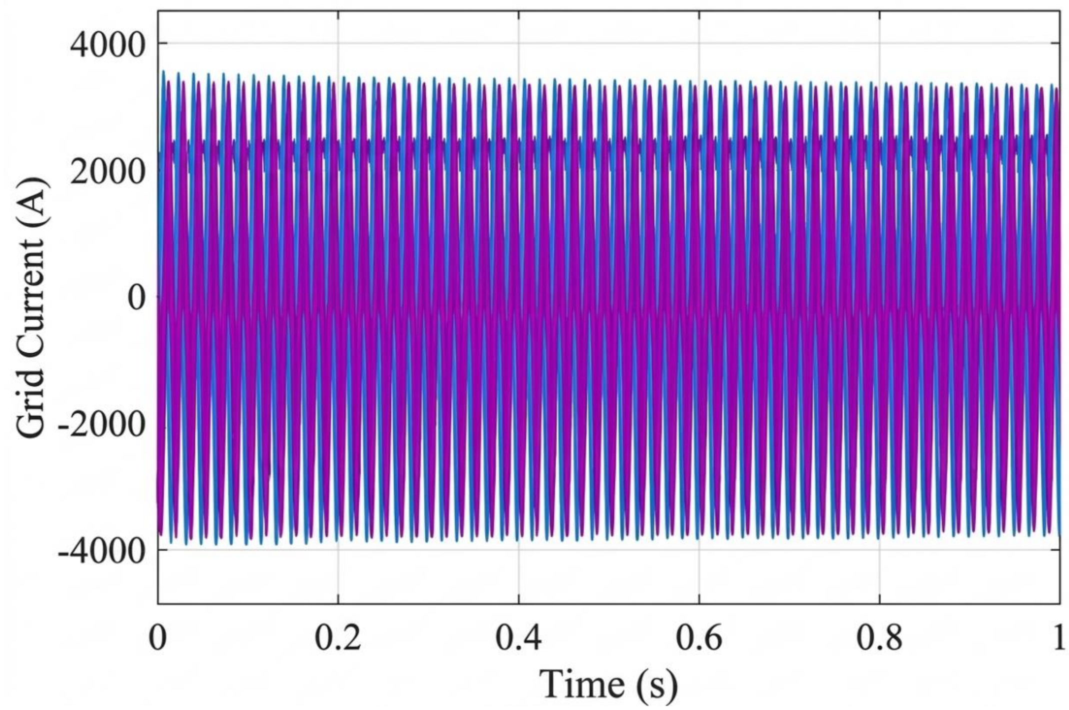

Fig. 9 Analysis for grid current

The waveform likely indicates the current flow between the grid and the connected system. Two waveforms indicate a plot of the current values of two phases of the grid connection and look sinusoidal, typical for AC power systems. The amplitudes of the waveforms are roughly 4000 amps. This would be the values at peaks, and means that it is the highest power that might have been asked from the grid-connected system. The frequency of the waveforms is roughly 50 Hz, which is the usual frequency for a power grid.

There is a phase difference between the two waveforms; this could also be a sign of a three-phase system, but with a well-balanced load. Waveforms are stable; the grid-connected system is in the state of steady flow. Figure 10 depicts the objective function of the proposed and conventional algorithms, like GOA (Grasshopper Optimization), PSO (Particle swarm optimization), SSA (Slap swarm algorithm), over 200 iterations.

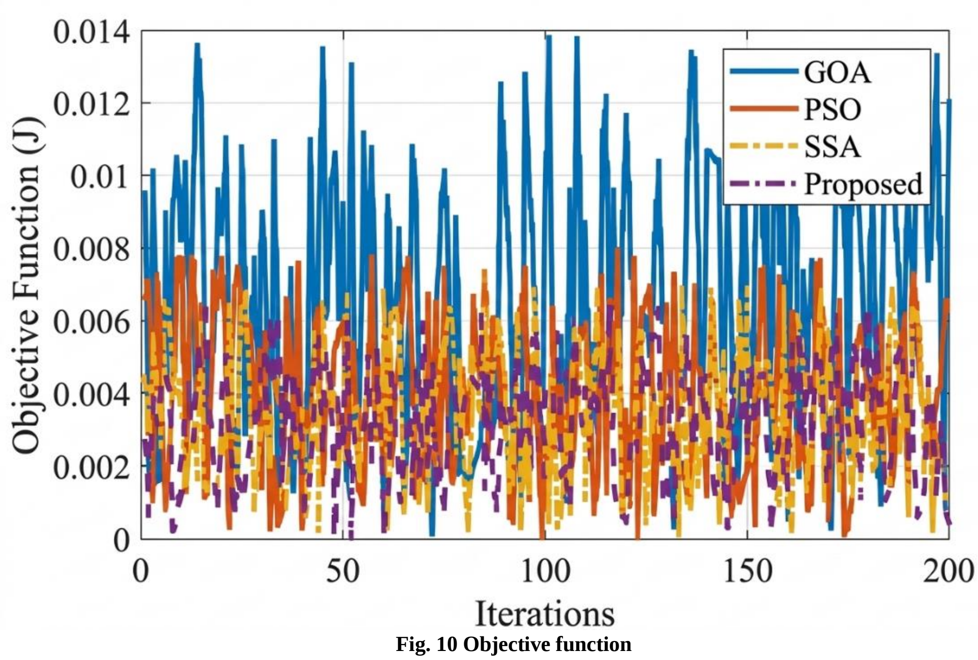

Fig. 10 Objective function

The GOA has variability with up to 0.014, so it has a relatively lesser optimal performance. The PSO stands in the middle with moderate variability peaking around 0.008. It performs better than GOA, but surely not the best among the ones. SSA remains lower than 0.006, so it has even lesser variability and, therefore, exhibits stable and efficient performances. The proposed method exhibits the least variability while it stays mostly below 0.004 values and remains even above all other methods for objective function minimization.

3.5. Comparison of THD

Figure 11 depicts the THD of the suggested method in addition to the control techniques. The harmonic suppression in this figure is 3.74% to the frequency of 60 Hz. Furthermore, it is well established that the method of VPPs incorporated by the proposed SA-STO is considerably more efficacious than the present standard FOPID, PID, as well as PI methods. The resulting SA-STO due to the Fractional Order PID controller reduces the power quality problems to a considerable extent.

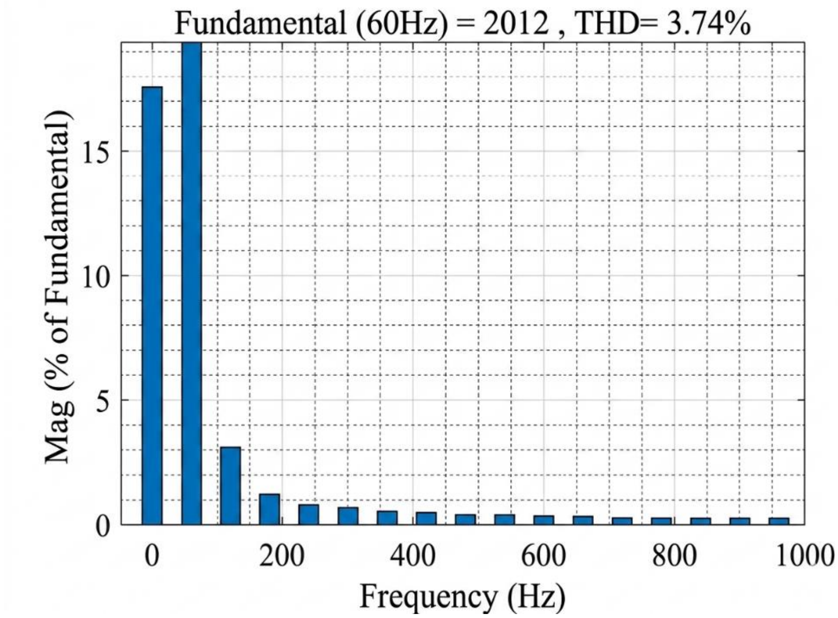

Fig. 11 THD analysis

The following figure is the bar graph for showing the harmonic contents of a signal; here, the x-axis is used to provide information about the frequency in Hertz or Hz, and the y-axis gives information about the magnitude of each harmonic content in percentage with respect to the fundamental. The fundamental component in this case has been at a frequency of 60 Hz, whose magnitude has been measured at 2012. The distortion level is relatively low at 3.74% THD. The plot of the magnitudes of the harmonic components from the second at 120 Hz up to the 17th at 1020 Hz illustrates quite effectively the frequency spectrum of the signal, as the strength of each harmonic component is depicted against the fundamental frequency. A comparison of the THD percentage using conventional techniques is tabulated in Table 2.

Table 2. Comparison of THD with existing approaches

Approaches	THD (%)	Peak Overshoot (Hz)	Power Loss (MW)	Settling Time (s)	Frequency Deviation (Hz)
PI	5.68	0.040	0.042	1.82	0.031
PID	4.62	0.037	0.034	1.54	0.026
FOPID	3.97	0.025	0.026	1.21	0.019
BWO-FOPID [20]	6.34	0.038	0.035	1.67	0.028
FOPID-COA [20]	12.15	0.034	0.028	1.43	0.023
AZQLMS and FOPID-FLO [21]	4.18	0.028	0.025	1.16	0.018
3DOF-PID [22]	3.98	0.025	0.018	0.98	0.014
Proposed SA-STO Hybrid PI-FOPID	3.74	0.020	0.013	0.74	0.010

Table 3. Statistical analysis comparison

Statistical Measure	THD (%)	Peak Overshoot (Hz)	Power Loss (MW)	Settling Time (sec)	Frequency Deviation
Mean	5.33	0.031	0.028	1.32	0.021
Median	4.4	0.031	0.027	1.32	0.021
Minimum	3.74	0.02	0.013	0.74	0.01
Maximum	12.15	0.04	0.042	1.82	0.031
Standard Deviation	2.67	0.007	0.009	0.34	0.007
Variance	7.13	0.00005	0.00008	0.12	0.00005

Given below, Table 3 shows the statistical significance test using standard deviation and mean error across different controller methods.

An analysis of the five-performance metrics indicates that THD is the metric with the greatest variation overall (mean = 5.33%, range 3.74% - 12.15%)). Peak Overshoot, Power Loss, Settling Time, and Frequency Deviation have moderate amounts of variation within those metrics (low standard deviation, consistent minimum value). All five of the above metrics have their lowest value associated with the Proposed controller, thereby demonstrating that the Proposed controller provides better power quality, stability, and efficiency than all other controllers. Figure 12 below shows the THD comparison analysis.

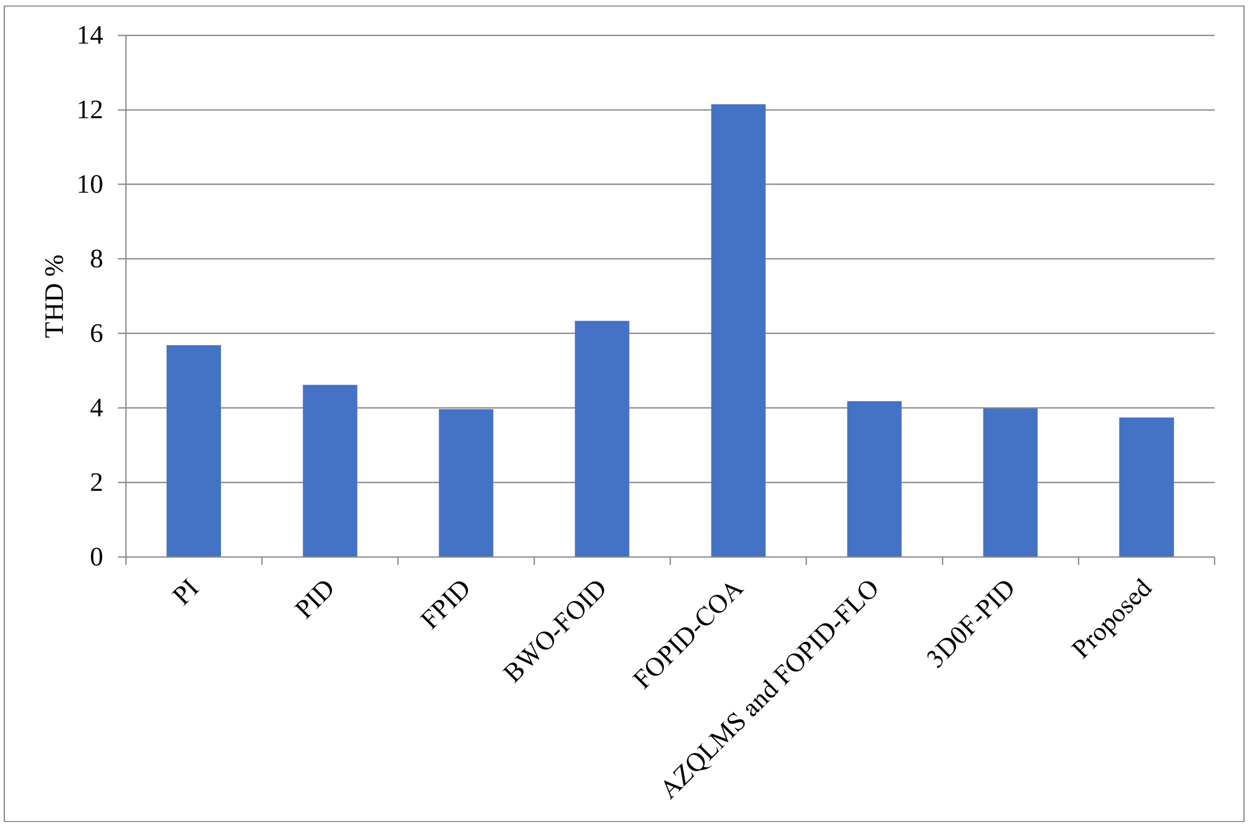

Fig. 12 THD comparison analysis

Figure 13 illustrates the overshoot analysis of the proposed and traditional controllers.

As shown in the figure, the Peak Overshoot (Hz) bar graph demonstrates that the PI controller has the highest peak overshoot at 0.040 (Hz), illustrating its relatively low/poor actual performance when compared to other controllers, while PID and BWO-FOID will have a high degree of similar peak overshoot. Conversely, the proposed controller has the lowest peak overshoot at approximately 0.020 (Hz), indicating that this controller has the best actual performance when compared to all controllers, thereby demonstrating its superior dynamic response characteristics and the most favourable ability to suppress peak overshoot. The power loss analysis of the proposed and conventional techniques is depicted in the Figure 14.

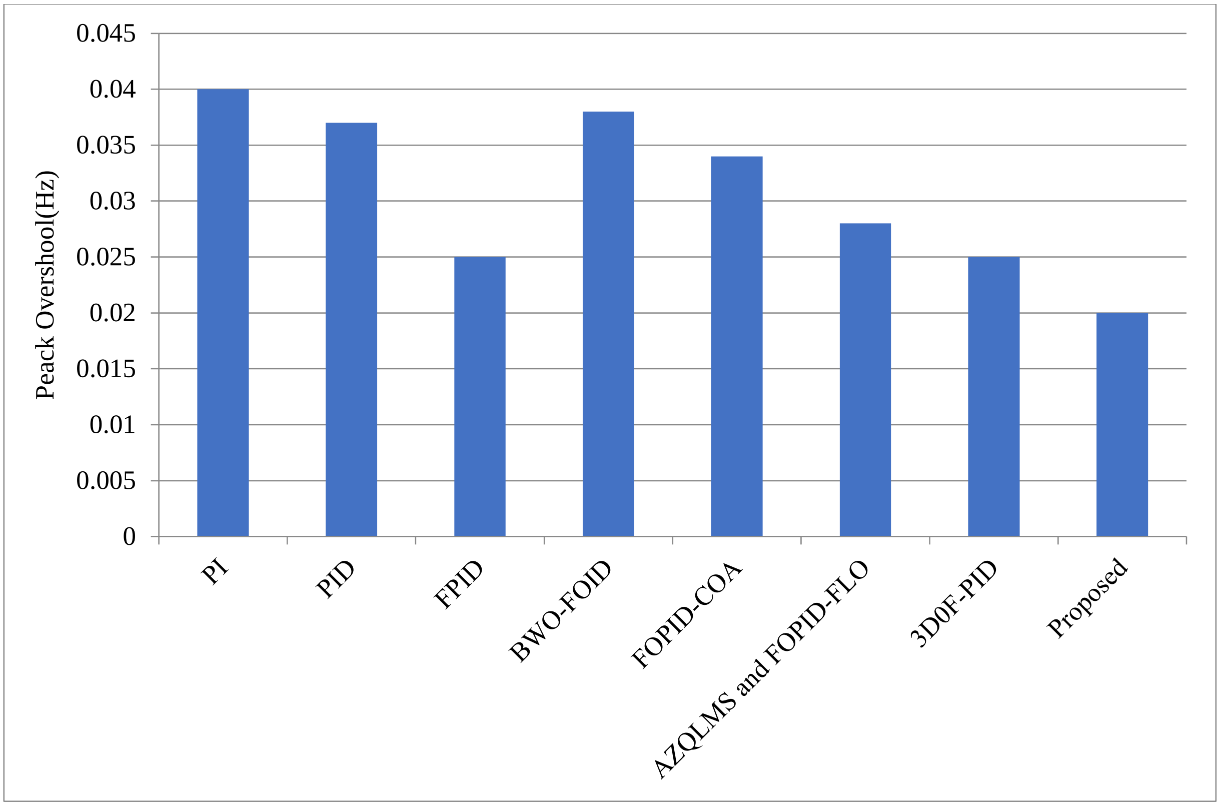

Fig. 13 Overshoot analysis

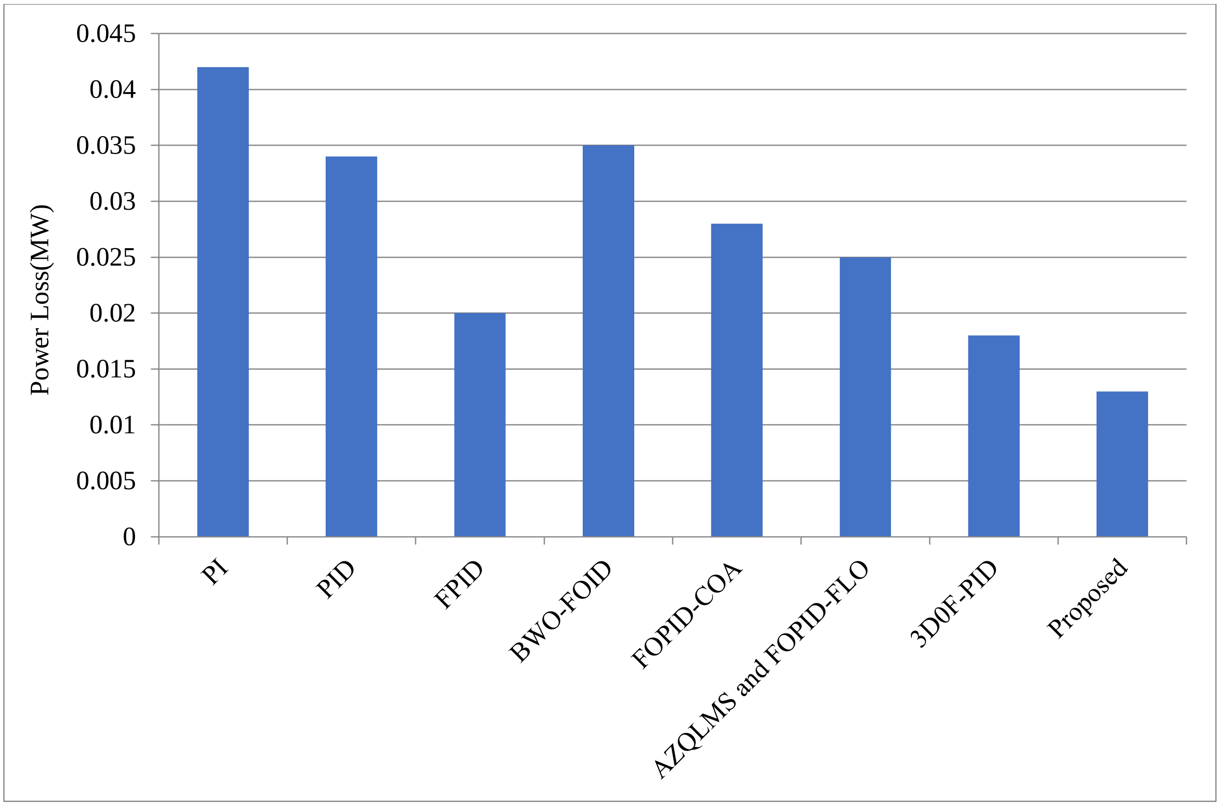

Fig. 14 Power loss analysis

The figure shows the six different controllers, which comparing the power loss (HZ). The PI controller had the largest power loss (approximately 0.042 MW); then, it is the least efficient; however, the PID and BWO-FOID also had relatively high-power losses. The proposed controller had the smallest power loss (approximately 0.013 MW); therefore, it is the most efficient at reducing power loss compared to any existing method.

Comparative Performance Analysis of Optimization Algorithms for VPP Control.

Table 4: Comparison of GA, DE, PSO, ABC, and SA-STO in terms of convergence speed, robustness, computational complexity, and limitations.

Table 4. Comparative analysis of optimization algorithm

Algorithm	Convergence Speed	Stability	Computational Complexity	Limitation
GA	0.72	0.80	0.78	Slow convergence
DE	0.81	0.86	0.65	Premature convergence
PSO	0.88	0.74	0.42	Local optima trapping
ABC	0.83	0.82	0.58	Weak exploitation capability
Proposed SA-STO	0.96	0.94	0.31	Improved adaptive optimization

The comparisons include consideration of the speed of convergence as well as robustness, computational complexity and any limitations. All comparisons were done using a normalized metric that ranged from 0 to 1. Higher values of the metrics indicate greater convergent speed or the robustness of the algorithm, whereas lower ratings indicate lower computational complexity.

The results showed that the SA-STO algorithm is stronger than the previous algorithms with regard to speed of convergence (more quickly), robustness, and computational complexity (less). Therefore, the SA-STO algorithm provides an appropriate algorithm to meet the requirements of optimal control of VPPs.

4. Conclusion

This research presented an SA-STO optimized hybrid PI-FOPID controller for Virtual Power Plant (VPP) applications to improve frequency regulation, minimize power losses, and enhance system stability under renewable energy fluctuations. The proposed hybrid controller combines the fast dynamic response of the PI controller with the robustness and flexibility of the FOPID controller to effectively handle nonlinear and uncertain operating conditions in VPP systems. The SA-STO algorithm was utilized to optimally tune the controller parameters for achieving improved dynamic performance and efficient energy management.

The obtained results demonstrated superior performance compared with conventional PI, PID, and FOPID controllers, where the Total Harmonic Distortion (THD) was reduced from 5.5% for PI, 5.0% for PID, and 4.2% for FOPID controllers to 3.74% using the proposed SA-STO-based hybrid PI-FOPID controller. In addition, the proposed method effectively reduced frequency deviations, improved power quality, minimized power losses, and enhanced the operational stability of the VPP under varying renewable energy conditions. Although the proposed methodology achieved better control performance, the optimization process increases computational complexity during real-time implementation in large-scale VPP systems.

4.1. Limitations and Future Work

In future studies, there will be an emphasis on overcoming practical challenges that must be solved in order to implement the SA-STO optimized hybrid PI-FOPID controller in Virtual Power Plants (VPP) within the real world. A key concern is the effect of communication delays between the Distributed Energy Resources (DERS) and the centralized control units on the overall system performance. Poor communication can result in a performance that is unstable or has poor dynamic response time. With regard to the physical limitations of the embedded controllers used to implement the SA-STO optimization algorithm, there will be related concerns regarding memory and processing power that affect the real-time implementation of the algorithm. Future research will explore the development of alternative optimization algorithms that provide computationally efficient ways of determining optimal PI-FOPID controller parameter values, including decentralized or distributed control frameworks and advanced communication techniques. The end goal of these efforts is to ensure reliable, scalable, and robust performance when the SA-STO optimized PI-FOPID controller is implemented in real-world VPP applications.

Funding

On Behalf of all authors, the corresponding author states that they did not receive any funds for this project.

Conflicts of Interest

The authors declare that we have no conflict of interest.

Acknowledgments

The authors would like to thank the Deanship of GITAM Deemed to be University for supporting this work.

References

[1] Weilin Zhong et al., "Coordinated Control of Virtual Power Plants to Improve Power System Short-Term Dynamics," *Energies*, vol. 14, no. 4, pp. 1-14, 2021. [CrossRef] [Google Scholar] [Publisher Link]

[2] Huangjie Gong et al., "Virtual Power Plant Control for Large Residential Communities using HVAC Systems for Energy Storage," *IEEE Transactions on Industry Applications*, vol. 58, no. 1, pp. 622-633, 2022. [CrossRef] [Google Scholar] [Publisher Link]

[3] Saeed Abrisham Foroushan Asl et al., "A New Two-Layer Model for Energy Management in the Smart Distribution Network Containing a Flexi-Renewable Virtual Power Plant," *Electric Power Systems Research*, vol. 194, pp. 1-10, 2021. [CrossRef] [Google Scholar] [Publisher Link]

[4] Jibin Kuriakose et al., "Virtual Power Plants in Coastal Environments: A Comprehensive Review of Technical Challenges and Mitigation Approaches," *Energy Conversion and Management: X*, vol. 30, pp. 1-34, 2026. [CrossRef] [Google Scholar] [Publisher Link]

[5] Huichuan Liu, Jing Qiu, and Junhua Zhao, "A Data-Driven Scheduling Model of Virtual Power Plant using Wasserstein Distributionally Robust Optimization," *International Journal of Electrical Power and Energy Systems*, vol. 137, 2022. [CrossRef] [Google Scholar] [Publisher Link]

[6] Liwei Ju et al., "Data-Driven Two-Stage Robust Optimization Dispatching Model and Benefit Allocation Strategy for a Novel Virtual Power Plant Considering Carbon-Green Certificate Equivalence Conversion Mechanism," *Applied Energy*, vol. 362, 2024. [CrossRef] [Google Scholar] [Publisher Link]

[7] Mohamed. A. Abdelghany et al., "Load Frequency and Virtual Inertia Control for Power System using Fuzzy Self-Tuned PID Controller with High Penetration of Renewable Energy," *Journal of Electrical Systems and Information Technology*, vol. 11, no. 1, 2024. [CrossRef] [Google Scholar] [Publisher Link]

[8] S. Dheenathayalan et al., "Optimized TDMA Framework for Channel Interference Mitigation in IWSN based on Self-Adaptive Affinity Propagation Clustering," *Optical and Quantum Electronics*, vol. 56, no. 12, 2024. [CrossRef] [Google Scholar] [Publisher Link]

[9] Reza Shahouni et al., "Adaptive Tuning of Fractional Order PID Controllers for Nonlinear Processes using Hybrid PSO DQN Reinforcement Learning," *Scientific Reports*, vol. 15, no. 1, pp. 1-24, 2025. [CrossRef] [Google Scholar] [Publisher Link]

[10] Ashtabhuj Kumar Srivastava et al., "Analysis of GOA Optimized Two-Stage Controller for Frequency Regulation of Grid-Integrated Virtual Power Plant," *Energy Reports*, vol. 8, pp. 493-500, 2022. [CrossRef] [Google Scholar] [Publisher Link]

[11] Maher G. M. Abdolrasol et al., "Energy Management Scheduling for Microgrids in the Virtual Power Plant System using Artificial Neural Networks," *Energies*, vol. 14, no. 20, pp. 1-19, 2021. [CrossRef] [Google Scholar] [Publisher Link]

[12] R. Abishek et al., "Frequency Control Strategy for Grid-Tied Virtual Power Plant using SSA-Tuned Fractional Order PID Controller," *IETE Journal of Research*, vol. 70, no. 3, pp. 2802-2818, 2023. [CrossRef] [Google Scholar] [Publisher Link]

[13] Wen Chen et al., "Bargaining Game-based Profit Allocation of a Virtual Power Plant in Frequency Regulation Market Considering Battery Cycle Life," *IEEE Transactions on Smart Grid*, vol. 12, no. 4, pp. 2913-2928, 2021. [CrossRef] [Google Scholar] [Publisher Link]

[14] Peng Bao, Wen Zhang, and Yuxi Zhang, "Secondary Frequency Control Considering Optimized Power Support from a Virtual Power Plant Containing Aluminum Smelter Loads Through the VSC-HVDC Link," *Journal of Modern Power Systems and Clean Energy*, vol. 11, no. 1, pp. 355-367, 2023. [CrossRef] [Google Scholar] [Publisher Link]

[15] Jannat Ul Ain Binte Wasif Ali et al., "Smart Energy Management in Virtual Power Plant Paradigm with a New Improved Multilevel Optimization-based Approach," *IEEE Access*, vol. 10, pp. 50062-50077, 2022. [CrossRef] [Google Scholar] [Publisher Link]

[16] Kanjanapon Borisoot et al., "Optimal Energy Management for Virtual Power Plant Considering Operation and Degradation Costs of Energy Storage System and Generators," *Energies*, vol. 16, no. 6, pp. 1-19, 2023. [CrossRef] [Google Scholar] [Publisher Link]

[17] Mohamed Lamari et al., "Multi-Objective Economic/Emission Optimal Energy Management System for Scheduling Micro-Grid Integrated Virtual Power Plant," *Energy Science and Engineering*, vol. 10, no. 8, pp. 3057-3074, 2022. [CrossRef] [Google Scholar] [Publisher Link]

[18] Poushali Pal et al., "IoT-based Real-Time Energy Management of Virtual Power Plant using PLC for Transactive Energy Framework," *IEEE Access*, vol. 9, pp. 97643-97660, 2021. [CrossRef] [Google Scholar] [Publisher Link]

[19] Verena Häberle et al., "Control Design of Dynamic Virtual Power Plants: An Adaptive Divide-and-Conquer Approach," *IEEE Transactions on Power Systems*, vol. 37, no. 5, pp. 4040-4053, 2022. [CrossRef] [Google Scholar] [Publisher Link]

[20] B. Srikanth Goud et al., "Power Quality Improvement using Distributed Power Flow Controller with BWO-based FOPID Controller," *Sustainability*, vol. 13, no. 20, pp. 1-33, 2021. [CrossRef] [Google Scholar] [Publisher Link]

[21] Ganesh Kumar Budumuru et al., "Power Quality Enhancement using AZQLMS and Fractional Order PID-based Control Through Dynamic Voltage Restorer," *CPSS Transactions on Power Electronics and Applications*, vol. 10, no. 3, pp. 296-303, 2025. [CrossRef] [Google Scholar] [Publisher Link]

[22] Priyanka Gandhi M, and Senthil Kumar M, "Instrumentation Guided Power Quality Enhancement in Renewable Energy/Battery Integrated Microgrids By 3DOF-PID Controllers," *Journal of Instrumentation*, vol. 20, no. 10, 2025. [CrossRef] [Google Scholar] [Publisher Link]